

Wavelength Dependence of the Suppressed Ionization of Molecules in Strong Laser Fields

J. Durá,^{*,†} A. Grün,[†] P. K. Bates,[†] S. M. Teichmann,[†] T. Ergler,[†] A. Senftleben,[‡] T. Pflüger,[‡] C. D. Schröter,[‡] R. Moshhammer,[‡] J. Ullrich,[‡] A. Jaroń-Becker,[§] A. Becker,[§] and J. Biegert^{†,||}

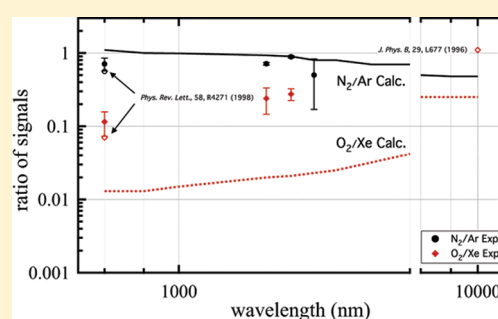
[†]ICFO-Institut de Ciències Fòniques, Av. Carl Friedrich Gauss 3, 08860 Castelldefels (Barcelona), Spain

[‡]Max-Planck-Institut für Kernphysik, Saupfercheckweg 1, 69117 Heidelberg, Germany

[§]JILA and Department of Physics, University of Colorado, UCB 440, Boulder 80309-0440, United States

^{||}ICREA-Institutio Catalana de Recerca i Estudis Avançats, 08010 Barcelona, Spain

ABSTRACT: We study ionization of molecules by an intense laser field over a broad wavelength regime, ranging from 0.8 to 1.5 μm experimentally and from 0.6 to 10 μm theoretically. A reaction microscope is combined with an optical parametric amplifier to achieve ionization yields in the near-infrared wavelength regime. Calculations are done using the strong-field *S*-matrix theory and agreement is found between experiment and theory, showing that ionization of many molecules is suppressed compared to the ionization of atoms with identical ionization potentials at near-infrared wavelengths at around 0.8 μm , but not at longest wavelengths (10 μm). This is due to interference effects in the electron emission that are effective at low photoelectron energies but tend to average out at higher energies. We observe the transition between suppression and nonsuppression of molecular ionization in the near-infrared wavelength regime (1–5 μm).



INTRODUCTION

Single ionization of atoms and molecules in intense laser fields, in particular in the tunneling regime (intensities above 10^{14} W/cm² at near-infrared wavelengths), has generated significant experimental and theoretical interest in the last decades. The phenomenon can be considered as the precursor of many other fundamental processes, such as above threshold ionization or high harmonic generation among others.^{1–5}

Ionization dynamics of atoms is nowadays very well understood,^{6–8} but an analysis of the same process in molecules is still under active experimental and theoretical research. Whereas in an atom the only channel in the matter–radiation interaction leading to disintegration of the bound system is ionization, in a molecule, ionization has to compete with many other open channels, such as dissociation, Coulomb explosion, dissociative ionization, or dissociative recombination among others. Even simple diatomic molecules can provide more information on dynamical aspects of strong field interaction than atoms due to the vast variety of electronic structures. Previous studies found experimentally that many ionization aspects of certain molecules in strong laser fields are similar to those of atoms with comparable ionization potential.^{9–12} For example, the pair N₂ and Ar, with similar ionization potentials $I_p(\text{N}_2) = 15.58$ eV and $I_p(\text{Ar}) = 15.76$ eV, shows very similar results in terms of the ionization yield as a function of laser intensity.^{10,12} Likewise, in the multiphoton ionization (MPI) regime the features in the photoelectron spectrum of N₂ are similar to multiphoton resonances in Ar.⁹ Similar behavior was found for CO molecule, $I_p(\text{CO}) = 14.01$ eV and

Kr, $I_p(\text{Kr}) = 14.00$ eV.^{11,54} This was understood in terms of tunneling ionization, where the ionization probability mainly depends on the ionization potential. A deviation from this trend was found at 0.8 μm for the pair O₂/Xe, where $I_p(\text{O}_2) = 12.07$ eV and $I_p(\text{Xe}) = 12.13$ eV; a strong suppression of the ionization of O₂, even more than an order of magnitude, was found compared to the Xe atom.^{12,13} Examples of this suppression phenomenon span from simple molecules, di- and triatomic^{12–16} over organic molecules^{16–18} up to complex molecules such as C₆₀.¹⁹ However, a set of experiments on molecular ionization using CO₂ lasers (operating at 10.6 μm)^{10,11} did not reveal any suppression of the ion yields of a series of di- and triatomic molecules as compared to the predictions for atomic tunnel ionization, in contrast to the observations at near-infrared wavelengths.

Most of the single ionization dynamics experiments were performed with Ti:sapphire laser systems at 0.8 μm ^{12,13} whereas some measurements were done, with longer pulse duration, at 10.6 μm with CO₂ lasers,^{10,11} but there is a gap between these two wavelength regimes. Recently, there has been an upsurge in the development of intense ultrashort laser pulses at wavelengths beyond 1 μm ^{20–22} driven by the scaling of strong field parameters

Special Issue: Femto10: The Madrid Conference on Femtochemistry

Received: July 29, 2011

Revised: October 18, 2011

Published: November 23, 2011

with the wavelength. An example is the ponderomotive (or cycle-averaged kinetic) energy of an oscillating electron $U_p \propto \lambda^2$. According to an established semiclassical picture^{23,24} an electron, which is removed by the field of the laser from an atom or molecule, can return to the parent ion in the oscillating field with a maximum kinetic energy of $3.17U_p$. The recollision of the electron leads to high-order harmonic and attosecond pulse generation,^{25,26} which can be used, for example, for molecular imaging.²⁷ In this context, an increase of the maximum kinetic energy by using longer laser wavelengths can lead to shorter attosecond pulses and radiation extending into the X-ray regime.

Intense long wavelength femtosecond laser sources will also enable more systematic investigations of phenomena which are seemingly well studied in the near-infrared wavelength regime. One example of such a phenomenon is the previously mentioned suppressed molecular ionization. Our laser sources, being tunable between 0.8 and 2.5 μm , help to elucidate ionization behavior on the largely uncovered range between 0.8 and 10.6 μm . This will advance the understanding of fundamental single ionization dynamics and consequently of the ionization suppression phenomena of molecules.

Parallel to the development of long wavelength sources, substantial theoretical effort has been put into the analysis of the suppression phenomenon mainly for the case of diatomic molecules at near-infrared wavelengths, based on S-matrix methods,^{28,29,31} numerical simulations of the time-dependent Schrödinger equation,^{32,33} tunnel ionization models,^{34,35} time-dependent density functional theory,^{36–39} and other models.^{40,41} From these studies it appears that multielectron effects,^{19,33,35,40,41} multicenter interference,^{28,29,31} and vibrational effects³² as well as nodal planes^{34,38} in molecular orbitals can cause a suppression of the electron emission from a molecule.

Here we present experimental results for the ratio of molecular-to-atomic ionization rates of the pairs N_2/Ar and O_2/Xe over the wavelength range from 0.8 to 1.5 μm . Ionization rates of the four different targets are measured as a function of laser intensity. This provides a route to investigate the trend of the ionization suppression phenomenon in the O_2 molecule with respect to Xe and the absence of suppression in N_2 with respect to Ar. All measurements are performed in the tunneling regime. Theoretical calculations for the same ratios of molecular-to-atomic ionization rates are presented here over the wavelength range from 0.6 to 10 μm . Di- and polyatomic, homo- and heteronuclear, and linear and cyclic molecules are included in the theoretical analysis to study the ionization ratio trends in a more general way.

THEORETICAL MODEL

We apply the well-known S-matrix formalism to obtain the total ionization rate of a molecule in a linearly polarized strong laser field as^{28–31} (Hartree atomic units with $e = m = \hbar = 1$ are used)

$$\Gamma_{\text{fi}}(I) = 2\pi N_e \int d\Omega_{\hat{n}} \sum_{N=N_0}^{\infty} k_N (U_p - N\omega)^2 \times \int d\hat{\mathbf{k}}_N J_N^2 \left(\alpha_0 \cdot \mathbf{k}_N, \frac{U_p}{2\omega} \right) \left| \langle \phi_{\mathbf{k}_N}(\mathbf{r}) | \phi_i(\mathbf{r}) \rangle \right|^2 \quad (1)$$

where N_e denotes the number of electrons in the active molecular orbital ϕ_i , $d\Omega_{\hat{n}}$ is the solid angle, \mathbf{k}_N is the electron momentum,

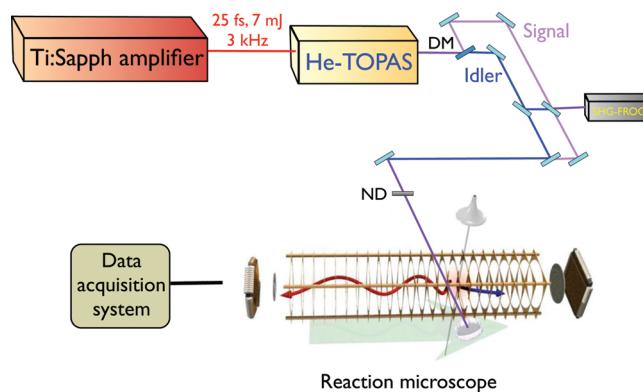


Figure 1. Schematic representation of the experimental setup. DM: dichroic mirror. SHG-FROG: second harmonic generation FROG system. ND: variable neutral density filter.

$\phi_{\mathbf{k}_N}$ is a plane wave, and \hat{n} is a unit vector along the main symmetry axis of the molecule. $J_N(a;b)$ is a generalized Bessel function of two arguments, where $\alpha_0 = I^{1/2}/\omega$ is the quiver radius and $U_p = I/4\omega^2$ is the ponderomotive energy of an electron in a laser field of frequency ω and intensity I . $k_N^2/2 = N\omega - U_p - I_p$ is the kinetic energy of the electron upon absorption of N photons from the field, I_p is the ionization potential, and N_0 is the minimum photon number which has to be absorbed to ionize the molecule.

Molecular wave functions, $\{\mathbf{R}_i\}$, which depend on the positions of the nuclei in the molecule, were obtained from the quantum chemical software package GAMESS-US,⁴² emission from different active orbitals are taken into account and the corresponding rates are incoherently added because the emission of electrons from different orbitals leads to different final states, distinguishable in energy of the electron, and therefore the different amplitudes cannot interfere. In the present calculations we drop the contributions from the nonactive electrons to the overlap matrix element in eq 1, because their effect on the total ionization rate is, in general, small. The results are obtained by averaging the ionization rate over the orientation of the molecule with respect to the laser polarization direction.

EXPERIMENTAL SECTION

The experimental setup is shown schematically in Figure 1.

Laser System. The Ti:sapphire system delivers 25 fs, 7 mJ pulses centered at 0.78 μm with a repetition rate of 3 kHz. The fundamental output is used to pump an optical parametric amplifier (Light Conversion, He-TOPAS) where a signal and idler pulses are generated in BBO crystals with wavelength tunability from 1.2 to 1.5 μm and from 1.7 to 2.5 μm , respectively. Both signal and idler are temporally characterized by a home-built second harmonic generation FROG (SHG-FROG) system,⁴³ which covers a wavelength range from 0.8 to 5 μm with up to 0.1 cm^{-1} resolution, and a temporal range of 100 ps with 0.12 fs resolution.

Many Particle Imaging Technique: Reaction Microscope. Experiments are performed using a reaction microscope; the principle has been extensively described in the literature.^{44–46} Briefly, the laser beam is focused by a spherical on-axis mirror ($f = 50$ mm) onto a low density supersonic gas-jet target ($\approx 1 \times 10^{11}$ atoms/ cm^3). The supersonic gas-jet is formed by expansion of the gas through a 30 μm nozzle. The stagnation pressure is set

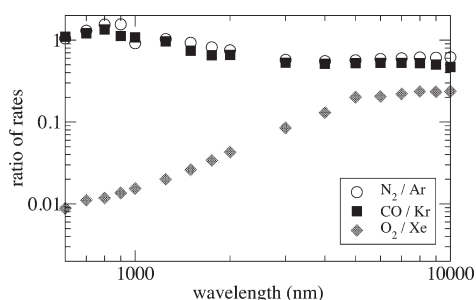


Figure 2. Ratios of ionization rates of diatomic molecules to those of companion atoms as a function of laser wavelength at $I = 10^{14} \text{ W/cm}^2$.

at 300 kPa and the pressure in the source chamber while running the jet is 40 mPa. Collimation of the molecular/atomic beam is achieved by 200 and 400 μm diameter skimmers. Differential pumping in three stages ensures a background pressure in the interaction chamber of $7 \times 10^{-8} \text{ Pa}$. A mass flow controller is used to guarantee the same gas density in the jet for the four different gases used.

Emitted recoiling ions and electrons created in the interaction region are extracted by small electric ($E \approx 3 \text{ V cm}^{-1}$) and magnetic fields ($B \approx 0.5 \text{ mTesla}$). Chevron configuration multichannel-plate (MCP) detectors with 80 mm diameters, mounted in opposite directions and perpendicular to the laser beam propagation, are used. The MCP detectors are equipped with delay line anodes for position encoding. The distance from the reaction volume to the detectors is symmetric for ions and electrons ($x = 15 \text{ cm}$). The solid angle acceptance for ions and electrons is nearly 4π , ensured for the latter by the magnetic field. Coincidence measurements of the time-of-flight (TOF) of the particles and their position on the detectors permit the reconstruction of the full initial momentum vector of the particles at the instant of the photoionization process, using the equations of motion for ions and electrons in a known electric and magnetic field.^{45–47}

Experimental Methodology. Cold particles of the molecular or atomic jet are ionized by the selected wavelength laser beam. The signal of the MCP detector is further amplified and discriminated, so that ions and electrons can be individually counted by the data acquisition system. The electron multiplier efficiency of the ions' MCP is proportional to $Z/M^{1/2}$,⁴⁸ where Z is the charge and M is the mass of the ion. Because the aim of the experiment is a comparison between ions with different masses, this factor needs to be taken into account in the final single ionization yield values; these are obtained by integration of the corresponding TOF ion signals over the exposure time, which could vary from 2×10^3 to 4×10^3 laser shots.

Absolute calibration of the laser intensity is needed for comparison of experiment and theory and to draw important conclusions from the data. The intensity is calibrated by fitting the Xe^+ ionization yield at different intensities of the fundamental Ti:sapphire output, to experimental and calculated ionization yields of Xe^+ under similar conditions and published elsewhere.¹² Knowing pulse duration and laser power, the final laser intensity on target can be set equal for the whole range of wavelengths studied.

RESULTS AND DISCUSSION

Theoretical Results. We first consider the three diatomic molecules N_2 , CO , and O_2 , which have ionization potentials similar to those of the three noble gas atoms Ar , Kr , and Xe ,

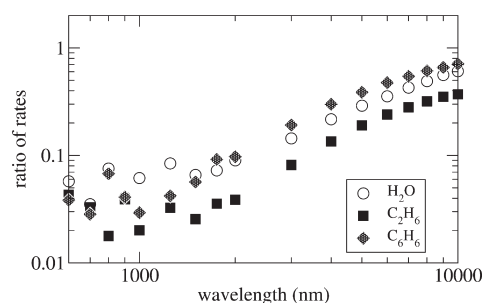


Figure 3. Same as Figure 2 but for the molecules H_2O , C_2H_6 , and C_6H_6 and their companion hydrogen-like atoms at $I = 3 \times 10^{13} \text{ W/cm}^2$.

respectively. Because we are interested in a comparative study, we calculate the S -matrix ionization rates of the atoms as well. This is easily done by replacing the molecular orbital in eq 1 in the initial state of the matrix element by the corresponding atomic orbital. There is no need for an averaging over the orientation of an atom with respect to the polarization direction. We determine the ratio of the molecular ionization rate to the atomic ionization rate as a function of the laser wavelength. The results, obtained at $I = 10^{14} \text{ W/cm}^2$, are shown in Figure 2.

For N_2 and CO we observe that the ratio varies over the whole range of wavelengths only slightly around 1, which indicates that there is no (significant) suppression of ionization for these molecules. At near-infrared wavelengths these results are in overall agreement with the observations in previous experiments, namely that N_2 ionization is almost not suppressed compared to Ar ^{12,14} whereas ion yields of CO show a slight suppression as compared to Kr .⁴⁹ Turning to longer wavelengths, the limit of the ratio for these two molecules is found to be about 0.6. As noted above, in the early experiments by Chin and co-workers at 10.6 μm no difference between the ion yields of a molecule and those of an atom was found.¹¹ This slight discrepancy without calculations could come from the lack of more sophisticated molecular wave functions and consideration of Coulomb effects in the final state calculations.

For O_2 the ratio of molecular-to-atomic ionization rates is by a factor of 100 below 1 at shorter wavelengths, which is in agreement with previous experiments for suppressed ionization.^{12,13} Interestingly, we observe that the ratio increases as a function of wavelength, in particular from 1 to 5 μm , until it converges to a value of about 0.2 at the longest wavelengths studied.

To investigate the dependence of the ratio of molecular to atomic ionization rate with wavelength, we consider three polyatomic molecules of different structures, namely H_2O , the linear hydrocarbon C_2H_6 and the aromatic hydrocarbon C_6H_6 . For the calculations of the rates of the companion atoms, the molecular matrix elements in eq 1 are replaced by those for hydrogen-like atoms having the same ionization potential as the respective molecule, leaving everything else unchanged. The corresponding ratios at $I = 3 \times 10^{13} \text{ W/cm}^2$ are shown in Figure 3 over the wavelength range from the visible to the infrared. In each case we find a suppression of the molecular ionization rate at visible and near-infrared laser wavelengths. But, as in the case of O_2 , the ratios steadily increase in the mid-infrared regime and approach the limit of nonsuppression, i.e., ratio of 1, at the longest wavelengths. The quantitative degree of suppression depends on the specific molecular structure and the symmetry of the molecular orbitals involved. However, the general trend appears to be analogous to that of O_2 .

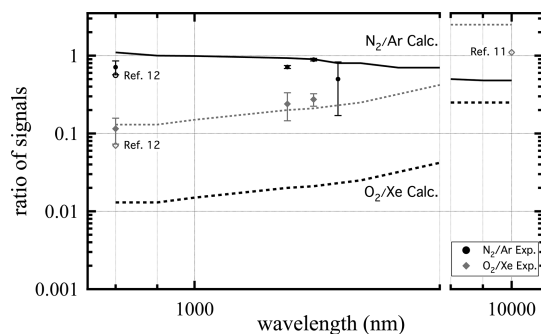


Figure 4. Ratios of ionization rates of diatomic molecules to those of companion atoms as a function of laser wavelength at $I = 10^{14} \text{ W/cm}^2$, numerical calculations, and $I = 3 \times 10^{13} \text{ W/cm}^2$, experimental results. Lines: numerical calculations (dash black, O_2/Xe ratio; dash gray, O_2/Xe ratio multiply by a factor 10; solid black, N_2/Ar ratio). Dots: experimental results (gray diamonds, O_2/Xe ratio; black circles, N_2/Ar ratio); error bars, standard deviation. Open dots: experimental results from literature.

Experimental Results. In this section we present results on the experimental single ionization yields of Ar, N_2 , Xe, and O_2 measured at four different wavelengths from 0.8 to 1.5 μm . Figure 4 shows measured as well as theoretical results as well as experimental data taken under similar experimental conditions from the literature.^{11,12}

Over the whole range of wavelengths the experimental N_2/Ar ratio is close to 1 and varies between 0.8 to 1.4 μm by less than 20%. This indicates that there is no single ionization suppression for the N_2 molecule, which is in good agreement with our calculations and with previous experiments at near-infrared wavelengths, where no suppressed ionization was found for N_2 relative to Ar.^{12,14} The experimental data taken under similar conditions by Guo et al.¹² are shown in Figure 4 as an open black circle at 0.8 μm .

The O_2/Xe single ionization ratio increases from ≈ 0.1 to ≈ 0.3 within the wavelength range 0.8–1.5 μm , which corresponds to an increase of more than a factor 2. Despite the fact that our experimental O_2/Xe results do not show a fully quantitative agreement with our calculated data, the qualitative transition from a strong suppression of ionization of O_2 at near-infrared wavelengths toward a much smaller suppression at infrared wavelengths is reflected in both the experimental observations and the numerical calculations. The discrepancy is a factor 10. Applying this scaling factor to the theoretical results, numerical calculations and experimental results agree quantitative and qualitatively. We will comment on the quantitative discrepancy between the experimental and theoretical data below. The suppressed single ionization observed at 0.8 μm is in agreement with previous experimental results,¹² shown as an open gray diamond in Figure 4. Note that the experimental data from Walsh et al.¹¹ at 10.6 μm , indicated as an open gray diamond in Figure 4 at that wavelength, manifest also a quantitative discrepancy with the calculations.

Discussion. Molecular single ionization suppression was first observed over ten years ago¹³ and has been extensively studied at around 0.8 μm for different molecules, from the most simple diatomic molecules to organic compounds.^{12,13,50–52} Likewise, substantial theoretical effort has been put into the analysis of the phenomenon.^{28,30,53,54} This work presents experimental and theoretical results for suppressed ionization from visible to mid-infrared

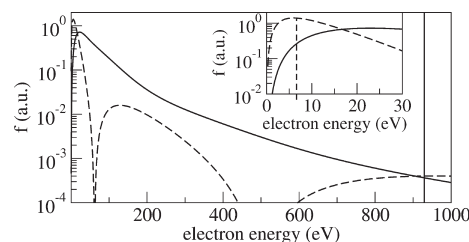


Figure 5. $f(E)$ (see text) as a function of electron energy E for O_2 (solid line) and Xe (dashed line). The inset shows an expanded view of the low energy part of the function. The vertical lines represent the ponderomotive energy U_p at an intensity of 10^{14} W/cm^2 at 0.8 μm (inset, dashed line) and 10 μm (main panel, solid line), respectively.

wavelengths. We observe the evolution of suppression toward nonsuppression for the O_2 molecule, as well as the almost linear trend of the ionization yield of N_2 . Our calculations reproduce the experimental observations found for N_2 qualitatively and quantitatively. The numerical results obtained for the pair O_2/Xe match qualitatively the experimental results but not quantitatively. The possible origin of the phenomenon together with the quantitative disagreement will be discussed in this section.

The first consistent explanation of the suppression phenomenon was given by Muth-Böhm et al. in terms of the symmetry of the highest occupied molecular orbital (HOMO), which induces a dynamical effect.²⁸ The HOMO symmetry is bonding- σ_g in the N_2 molecule and antibonding- π_g in O_2 . The electron density of the HOMO²⁸ is spatially differently distributed in an antibonding- π_g than in a bonding- σ_g orbital. In the antibonding symmetry there is no electron density in the central region of the diatomic molecule or along the molecular axis, whereas in the case of the bonding symmetry there is considerable electron density concentrated in those areas. This reflects the changes in the phase of the wave function in different regions. Thus, the σ_g symmetry results in a constructive interference between the two electron wave packets coming from the two atomic centers. In contrast, there is a destructive interference effect for emission of an electron from a π_g orbital, which leads to a suppression of the emitted electron from this type of orbital. Our experiments as well as numerical calculations at visible and near-infrared wavelengths are consistent with these symmetry considerations. Although there is no ionization suppression of the N_2 molecule, σ_g -HOMO, there is considerable suppression in the O_2 molecule, where the HOMO is π_g . Despite the HOMO symmetry being σ_g in the CO molecule, the heteronuclear character develop a slightly asymmetric molecular orbitals over the two atomic centers and therefore the constructive interference is not perfect.

This symmetry considerations alone cannot, however, explain neither the observed experimental and calculated trend of the ionization ratio in our work for the pair O_2/Xe nor the rest of theoretically studied molecules (H_2O , C_2H_6 , and C_6H_6), where the ratios increase as a function of wavelength toward the nonsuppression situation. Therefore, we use the strong-field S-matrix theory to gain further insights. The S-matrix calculation of the atomic and molecular ionization rates differ, for the most part, in the Fourier transform of the initial state wave function. We therefore present in Figure 5, the Fourier transform (integrated over the electron emission angle and the orientation of the molecular main symmetry axis)

$$f(E) = 2\pi N_e k \int d\hat{\Omega}_{\hat{n}} \times \int d\hat{k} |\langle \phi_k(\mathbf{r}) | \phi_i(\mathbf{r}) \rangle(\hat{n})|^2 \quad (2)$$

as a function of the electron energy $E = k^2/2$ for O_2 (solid line) and Xe (dashed line). In the atomic case the molecular wave function is replaced by the atomic one and the integral over the orientation is dropped in eq 2. The inset shows the low energy part of f and the vertical lines represent the ponderomotive energy U_p at an intensity of 10^{14} W/cm² for laser light at $0.8 \mu\text{m}$ (inset, dashed line) and $10 \mu\text{m}$ (main panel, solid line).

In the sum over N for the total ionization rate, eq 1, the most significant contributions arise from terms with $E_N \leq U_p$. The comparison in Figure 5 shows that for O_2 at $\lambda = 0.8 \mu\text{m}$ and $I = 10^{14}$ W/cm² $f(E)$ is suppressed relative to Xe in this energy range, because

$$f(E) \propto \sin^2(\mathbf{k} \cdot (\mathbf{R}_1 - \mathbf{R}_2)/2) \quad (3)$$

for electron emission from a π_g -orbital.²⁸ As a result, the low energy part of the electron energy spectrum as well as the total ionization rate is suppressed in the case of O_2 .

At larger energies the effect of the structure factor, eq 3, averages out because for the total rate there is an integration over $d\mathbf{k}$ and, in the case of a randomly oriented ensemble of molecules, another integration over $d\Omega_n$. For O_2 , $f(E)$ does therefore not show any further minima except for that near the threshold. Instead, the overall decrease of $f(E)$ is similar to that of the companion atom Xe. Please note that for Xe $f(E)$ exhibits the well-known Cooper minima at intermediate energies, which are not present in the case of O_2 . At mid-infrared wavelengths the energy regime that contributes to the sum of the total rate extends up to several hundreds of electronvolts (solid vertical line in the main panel of Figure 5). Therefore, the suppression of $f(E)$ in O_2 over the rather small energy range near threshold decreases as the wavelength increases and the total molecular ionization rate approaches that of the companion atom at long wavelengths.

The suppression of the differential ionization rate near threshold energies, i.e., photoelectron energies close to zero, for O_2 in the present theoretical predictions is stronger than in experimental above threshold ionization spectra⁵⁵ by a factor of about 10 (Figure 4). It has been recently shown⁵⁶ that the degree of suppression in the ionization rates of O_2 does depend on the inclusion of laser dressing effects in the initial state, the choice of gauge (length vs velocity)⁵⁷ as well as the Coulomb corrections in the final state.⁵⁸ The latter two corrections can introduce strong suppression as compared with experiments ranging from a factor of 2 to even a factor of 100,^{57,58} in agreement with the degree of quantitative discrepancy between theory and experiment in the present study. However, the general theoretical interpretation in view of interference effects given above still holds in these modified S-matrix theories.⁵⁶ Because these theories are not developed for the general case of a polyatomic molecule up to now, we restricted ourselves here to the original molecular strong field approximation (SFA) theory to theoretically analyze the effect of suppressed molecular ionization as a function of photon energy in general.

Indeed, the above qualitative interpretation for diatomic molecules holds for the general case as well. In a polyatomic molecule (partial) destructive interference between electron wave packets emerging from different atomic centers will contribute to a suppression of electron emission at low energies and will be most effective for the total ionization rates at optical and near-infrared wavelengths. Because any interference effect depends of the scalar product between the electron momentum vector and the position vectors of the atoms in the molecule, such

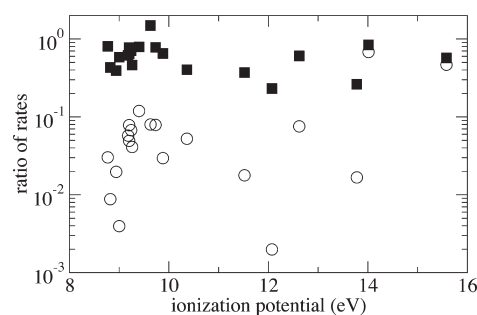


Figure 6. Ratios of ionization rates of a set of molecules to those of companion hydrogen-like atoms as a function of the ionization potential. Rates are obtained at $0.8 \mu\text{m}$ (open circles) and $10 \mu\text{m}$ (filled squares) at $I = 3 \times 10^{13}$ W/cm².

effects tend to average out at larger energies. Consequently, at long wavelengths, at which a broad energy spectrum contributes to the total rate, molecular ionization is expected to be non-suppressed. This not only is in agreement with the theoretical results in Figure 3 but also is theoretically predicted for an even larger set of molecules, including homo- as well as heteronuclear, linear as well as cyclic, symmetric as well as asymmetric molecules. This can be seen from the results in Figure 6, in which we compare the S-matrix predictions for the ratios of molecular to atomic ionization at $0.8 \mu\text{m}$ (open circles) with those at $10 \mu\text{m}$ (filled squares) at $I = 3 \times 10^{13}$ W/cm² for the diatomics N_2 (ionization potential: 15.58 eV), CO (14.01 eV), O_2 (12.07 eV), and NO (9.26 eV), the triatomics CO_2 (13.78 eV) and H_2O (12.62 eV), the hydrocarbons C_2H_6 (12.07 eV), C_3H_4 (11.52 eV), C_3H_6 (9.63 eV), C_6H_6 (9.24 eV), C_6H_{12} (9.4 eV), C_7H_8 (8.82 eV), and C_8H_{10} (8.77 eV), the fluorinated benzenes C_6H_5F (9.2 eV) and C_6HF_5 (9.63 eV), the chlorinated benzenes $C_6H_3Cl_3$ (9.18 eV) and $C_6H_4Cl_2$ (8.94 eV), and the biomolecules $C_4H_4N_2O_2$ (9.2 eV) and $C_5H_6N_2O_2$ (9.0 eV). As can be seen from the comparison, except for N_2 and CO, we find a suppression of the molecular ionization rate at the near-infrared wavelength, which is in general agreement with recent experiments.^{17,18} In contrast, the degree of suppression, if any, is much smaller at the infrared wavelength. Please note that our discussion is based on theoretical ionization rates for molecules randomly oriented with respect to the polarization axis and therefore does not account for the effect of a possible dynamic alignment of the specific molecule during the pulse. In the case of diatomic molecules it has been found that dynamic alignment occurs in pulses of 50 fs and longer.^{59,60} Thus, we expect that the present predictions hold for ionization yields, to be obtained via solution of the rate equations, in ultrashort pulses, as used in the present experiment. For longer pulses, in which dynamic alignment and ionization may coexist, one would need to consider ionization rates, averaged over certain alignment angles⁶¹ in the rate equations.

CONCLUSION

In conclusion, we have studied suppressed molecular ionization over a broad laser wavelength regime experimentally as well as theoretically, from the visible to the infrared. Experimentally, we have investigated the pairs N_2/Ar and O_2/Xe as molecules and atoms with similar ionization potentials. To obtain a general understanding of the phenomenon, numerical calculations have been performed in a large set of molecules. Our results, obtained using the strong-field S-matrix theory, are in qualitative agreement with the experimental

results shown in this work as well as recent experimental data at near-infrared and infrared laser wavelengths.^{10–13} For almost all molecules we have found a transition from a suppression of the rate of ionization of the molecule (as compared to that of a companion atom) at short wavelengths to a nonsuppression at long wavelengths. The transition occurs in the near and mid-infrared wavelength regime, which has been accessible in these experiments for the first time, to the best of our knowledge. Theoretical analysis shows that the suppression is due to an interference effect in the electron emission which is effective only at low photon energies.

AUTHOR INFORMATION

Corresponding Author

*E-mail: judith.dura@icfo.es.

ACKNOWLEDGMENT

The CU theory team thanks Prof. S. L. Chin for his interest in this work and his encouragement. This work was partially supported by U.S. National Science Foundation. We acknowledge support from the Spanish Ministerio de Ciencia e Innovación (MICINN) through its Consolider Program (SAUUL-CSD 2007-00013), “Plan Nacional” (FIS2008-06368-C02-01) and the Catalan Agència de Gestió d'Ajuts Universitaris i de Recerca (AGAUR) with SGR 2009-2013. Funding from LASERLAB-EUROPE(228334) is gratefully acknowledged. J.D. was partially supported by FONCICYT Project 94142.

REFERENCES

- (1) Agostini, P.; Fabre, F.; Mainfray, G.; Petite, G.; Rahman, N. K. *Phys. Rev. Lett.* **1979**, *42*, 1127.
- (2) McPherson, A.; Gibson, G.; Jara, H.; Johann, U.; Luk, T. S.; McIntyre, I. A.; Boyer, K.; Rhodes, C. K. *J. Opt. Soc. Am. B* **1987**, *4*, 595.
- (3) Bandrauk, A. D., Ed. *Molecules in Laser Fields*; Marcel Dekker: New York, 1994.
- (4) Bellini, M.; Lyngå, C.; Tozzi, A.; Gaarde, M. B.; Hänsch, T. W.; L'Huillier, A.; Wahlström, C. G. *Phys. Rev. Lett.* **1998**, *81*, 297.
- (5) Posthumus, J., Ed. *Molecules and Clusters in Intense Laser Fields*; Cambridge University Press: Cambridge, U.K., 2001.
- (6) August, S.; Strichland, D.; Meyerhofer, D. D.; Chin, S. L.; Heberly, J. H. *Phys. Rev. Lett.* **1989**, *63*, 2212.
- (7) August, S.; Meyerhofer, D. D.; Strichland, D.; Chin, S. L.; Heberly, J. H. *J. Opt. Soc. Am. B* **1991**, *8*, 858.
- (8) Walker, B.; Sheehy, B.; DiMauro, L. F.; Agostini, P.; Schafer, K. J.; Kulander, K. C. *Phys. Rev. Lett.* **1994**, *73*, 1227.
- (9) Gibson, G. N.; Freeman, R. R.; McIlrath, T. J. *Phys. Rev. Lett.* **1991**, *67*, 2492.
- (10) Chin, S. L.; Liang, Y.; Decker, J. E.; Ilkov, F. A.; Ammoscov, M. V. *J. Phys. B* **1992**, *25*, L249.
- (11) Walsh, T. D. G.; Decker, J. E.; Chin, S. L. *J. Phys. B* **1993**, *26*, L85. Walsh, T. D. G.; Decker, J. E.; Chin, S. L. *J. Phys. B* **1994**, *27*, 3767.
- (12) Guo, C.; Li, M.; Nibarger, J. P.; Gibson, G. N. *Phys. Rev. Lett.* **1998**, *81*, R4271.
- (13) Talebpour, A.; Chien, C. Y.; Chin, S. L. *J. Phys. B* **1996**, *29*, L677. Talebpour, A.; Larochelle, S.; Chin, S. L. *J. Phys. B* **1998**, *31*, L49.
- (14) Talebpour, A.; Yang, J.; Chin, S. L. *Opt. Commun.* **1999**, *163*, 29.
- (15) DeWitt, M. J.; Wells, E.; Jones, R. R. *Phys. Rev. Lett.* **2001**, *81*, 153001. Wells, E.; DeWitt, M. J.; Jones, R. R. *Phys. Rev. Lett.* **2002**, *66*, 013409.
- (16) Talebpour, A.; Larochelle, S.; Chin, S. L. *J. Phys. B* **1998**, *31*, 2769. Talebpour, A.; Bandrauk, A. D.; Yang, J.; Chin, S. L. *Chem. Phys. Lett.* **1999**, *313*, 789.
- (17) Hankin, S. M.; Villeneuve, D. M.; Corkum, P. B.; Rayner, D. M. *Phys. Rev. Lett.* **2000**, *84*, 5082. Hankin, S. M.; Villeneuve, D. M.; Corkum, P. B.; Rayner, D. M. *Phys. Rev. Lett.* **2001**, *64*, 013405.
- (18) Harada, H.; Tanaka, M.; Murakami, M.; Shimizu, S.; Yatsushashi, T.; Nakashima, N.; Sakabe, S.; Izawa, Y.; Tojo, S.; Majima, T. *J. Phys. Chem. A* **2003**, *107*, 6580.
- (19) Bhardwaj, V. R.; Corkum, P. B.; Rajner, D. M. *Phys. Rev. Lett.* **2003**, *91*, 203004.
- (20) Shan, B.; Chang, Z. *Phys. Rev. A* **2001**, *65*, 011804(R).
- (21) Colomiso, P.; et al. *Nat. Phys.* **2008**, *4*, 386.
- (22) Popmintchev, T.; Chen, M. C.; Cohen, O.; Grisham, M. E.; Rocca, J. J.; Murnane, M. M.; Kapteyn, H. C. *Opt. Lett.* **2008**, *33*, 2128.
- (23) Schafer, K. J.; Yang, B.; DiMauro, L. F.; Kulander, K. C. *Phys. Rev. Lett.* **1993**, *70*, 1599.
- (24) Corkum, P. B. *Phys. Rev. Lett.* **1993**, *71*, 1994.
- (25) Agostini, P.; DiMauro, L. F. *Rep. Prog. Phys.* **2004**, *67*, 813.
- (26) Corkum, P. B.; Krausz, F. *Nat. Phys.* **2007**, *3*, 381.
- (27) Itatani, J.; Levesque, J.; Zeidler, D.; Niikura, H.; Pepin, H.; Kieffer, J. C.; Corkum, P. B.; Villeneuve, D. M. *Nature* **2004**, *432*, 867.
- (28) Muth-Böhm, J.; Becker, A.; Faisal, F. H. M. *Phys. Rev. Lett.* **2000**, *85*, 2280. Erratum. *Phys. Rev. Lett.* **2006**, *96*, 039902.
- (29) Muth-Böhm, J.; Becker, A.; Chin, S. L.; Faisal, F. H. M. *Chem. Phys. Lett.* **2001**, *337*, 313.
- (30) Jaroń-Becker, A.; Becker, A.; Faisal, F. H. M. *Phys. Rev. A* **2004**, *69*, 023410.
- (31) Jaroń-Becker, A.; Becker, A.; Faisal, F. H. M. *Phys. Rev. Lett.* **2006**, *96*, 14006. Jaroń-Becker, A.; Becker, A.; Faisal, F. H. M. *J. Chem. Phys.* **2007**, *126*, 124310.
- (32) Saenz, A. J. *Phys. B* **2000**, *33*, 4365.
- (33) Wu, J.; Guo, C. *Adv. Studies Theor. Phys.* **20082**, *2*, 271.
- (34) Tong, X. M.; Zhao, Z. X.; Lin, C. D. *Phys. Rev. Lett.* **2002**, *66*, 033402.
- (35) Brabec, T.; Cote, M.; Boulanger, P.; Ramunno, L. *Phys. Rev. Lett.* **2005**, *95*, 073001.
- (36) Chu, X.; Chu, S. I. *Phys. Rev. A* **2004**, *70*, 061402(R).
- (37) Dundas, D.; Rost, J. M. *Phys. Rev. A* **2005**, *71*, 013421.
- (38) Otobe, T.; Yabana, K. *Phys. Rev. A* **2007**, *75*, 062507.
- (39) Usachenko, V. I.; Pyak, P. E.; Kim, V. V. *Phys. Rev. A* **2009**, *79*, 023415.
- (40) Guo, C. *Phys. Rev. Lett.* **2000**, *85*, 2276.
- (41) Lezius, M.; Blanchet, V.; Rayner, D. M.; Villeneuve, D. M.; Stolow, A.; Ivanov, M. Y. *Phys. Rev. Lett.* **2001**, *86*, 51.
- (42) Schmidt, M. W.; et al. *J. Comput. Chem.* **1993**, *14*, 1347.
- (43) Bates, P. K.; Chalus, O.; Biegert, J. *Opt. Lett.* **2010**, *35*, 1377.
- (44) de Jesus, V. L. B.; Rudenko, A.; Feuerstein, B.; Zrost, K.; Schröter, C. D.; Moshhammer, R.; Ullrich, J. *J. Electron. Spectrosc.* **2004**, *141*, 127.
- (45) Dörner, R.; Mergel, V.; Jagutzki, O.; Spielberger, L.; Ullrich, J.; Moshhammer, R.; Schmidt-Böcking, H. *Phys. Rep.* **2000**, *330*, 95.
- (46) Ullrich, J.; Moshhammer, R.; Dorn, A.; Dörner, R.; Schmidt, L. P. H.; Schmidt-Böcking, H. *Rep. Prog. Phys.* **2003**, *66*, 1463.
- (47) Ullrich, J.; Shevelko, V. P., Eds. *Matter-Particle Quantum Dynamics in Atomic and Molecular Fragmentation*; Springer-Verlag: Heidelberg, 2003.
- (48) Cornaggia, C.; Lavancier, J.; Normand, D.; Morellec, J.; Agostini, P.; Chambaret, J. P.; Antonetti, A. *Phys. Rev. A* **1991**, *44*, 4499.
- (49) Talebpour, A. *Ph.D. Thesis*, Université Laval, Québec, 1998.
- (50) Hankin, S. M.; Villeneuve, D. M.; Corkum, P. B.; Rayner, D. M. *Phys. Rev. Lett.* **1999**, *84*, 5082.
- (51) Hankin, S. M.; Villeneuve, D. M.; Corkum, P. B.; Rayner, D. M. *Phys. Rev. A* **2001**, *64*, 5082.
- (52) Litvinyuk, I. V.; Lee, K. F.; Dooley, P. W.; Rayner, D. M.; Villeneuve, D. M.; Corkum, P. B. *Phys. Rev. A* **2003**, *64*, 13405.
- (53) Kjeldsen, T. K.; Madsen, L. B. *Phys. Rev. A* **2005**, *71*, 023411.
- (54) Jaroń-Becker, A.; Becker, A. *Laser Phys.* **2009**, *19*, 1705.
- (55) Grasbon, F.; Paulus, G. G.; Chin, S. L.; Walther, H.; Muth-Böhm, J.; Becker, A.; Faisal, F. H. M. *Phys. Rev. A* **2001**, *63*, 041402(R).
- (56) Busuladzic, M.; Milosevic, D. B. *Phys. Rev. A* **2010**, *82*, 015401.
- (57) Kjeldsen, T. K.; Madsen, L. B. *Phys. Rev. A* **2004**, *71*, 023411.

- (58) Larochele, S. F. J.; Talebpour, A.; Chin, S. L. *J. Phys. B: At. Mol. Opt. Phys.* **1998**, *31*, 1215.
- (59) Voss, S.; Alnaser, A. S.; Tong, X. M.; Maharjan, C.; Ranitovic, P.; Ulrich, B.; Shan, B.; Chang, Z.; Lin, C. D.; Cocke, C. L. *J. Phys. B* **2004**, *37*, 4239.
- (60) Huang, J.; Wu, C.; Xu, N.; Liang, Q.; Wu, Z.; Yang, H.; Gong, Q. *J. Phys. Chem. A* **2006**, *110*, 10179.
- (61) Jaron-Becker, A.; Becker, A.; Faisal, F. H. M. *J. Phys. B* **2003**, *36*, L375.